J Mol Model (2011) 17:3085–3102
DOI 10.1007/s00894-011-0999-2

ORIGINAL PAPER

Quantum-chemical study of interactions of *trans*-resveratrol with guanine-thymine dinucleotide and DNA-nucleobases

Damian Mikulski · Małgorzata Szeląg · Marcin Molski

Received: 15 September 2010 / Accepted: 28 January 2011 / Published online: 1 March 2011

Abstract *Trans*-resveratrol, a natural phytoalexin present in red wine and grapes, has gained considerable attention because of its antiproliferative, chemopreventive and proapoptotic activity against human cancer cells. The accurate quantum-chemical computations based on the density functional theory (DFT) and *ab initio* second-order Møller-Plesset perturbation method (MP2) have been performed for the first time to study interactions of *trans*-resveratrol with guanine-thymine dinucleotide and DNA-derived nitrogenous bases: adenine, guanine, cytosine and thymine in vacuum and water medium. This compound is found to show high affinity to nitrogenous bases and guanine-thymine dinucleotide. The electrostatic interactions from intermolecular hydrogen bonding increase the stability of complexes studied. In particular, significantly strong hydrogen bonds between 4′-H atom of *trans*-resveratrol and imidazole nitrogen as well as carbonyl oxygen atoms of nucleobases studied stabilize these systems. The stabilization energies computed reveal that the negatively charged *trans*-resveratrol-dinucleotide complex is more energetically stable in water medium than in vacuum. MP2 method gives more reliable and significantly high values of stabilization energy of *trans*-resveratrol-dinucleotide, *trans*-resveratrol-guanine and *trans*-resveratrol-thymine complexes than B3LYP exchange-correlation functional because it takes into account London dispersion energy. According to the results, in the presence of *trans*-resveratrol the 3′-5′ phosphodiester bond in dinucleotide can be cleaved and the proton from 4′-OH group of *trans*-resveratrol migrates to the 3′-O atom of dinucleotide. It is concluded that *trans*-resveratrol is able to break the DNA strand. Hence, the findings obtained help understand antiproliferative and anticancer properties of this polyphenol.

Keywords DFT method · Dinucleotide · MP2 method · Nitrogenous base · Trans-resveratrol

Electronic supplementary material The online version of this article (doi:10.1007/s00894-011-0999-2) contains supplementary material, which is available to authorized users.

D. Mikulski (✉) · M. Szeląg · M. Molski
Department of Theoretical Chemistry, Faculty of Chemistry,
A. Mickiewicz University ul,
Grunwaldzka 6,
60-780 Poznań, Poland
e-mail: dmkwant@amu.edu.pl

M. Szeląg
Faculty of Biology, A. Mickiewicz University ul,
Umultowska 89,
61-614 Poznań, Poland

Introduction

Trans-resveratrol (*trans*-4′,3,5-trihydroxystilbene, TR, Fig. 1) is a natural polyphenolic derivative of *trans*-stilbene. It is found in significant levels in grapes, mulberries and peanuts. In small amounts it is also present in red wine. Many authors have proved that TR exhibits anti-inflammatory [1], anti-platelet [2], anti-mutagenic [3] and antioxidant [4] activity. Hence, this compound plays an important role in protection against carcinogenesis, inflammation, coronary heart disease and arteriosclerosis. TR has been identified as the anticancer agent that suppresses three major stages of carcinogenesis - initiation, promotion and progression [1]. Additionally, TR has gained wide attention of scientists because it has shown inhibitory effect in the interactions with vascular NADH/NADPH oxidase [5], cyclooxygenase COX-1 [6], ribonucleotide reductase [7] and DNA polymerase [8]. Inhibitory action of TR against the low-density lipoprotein (LDL) oxidation by copper ions (II) was presented by Frankel et al. [9]. Belguendouz et al. [10]

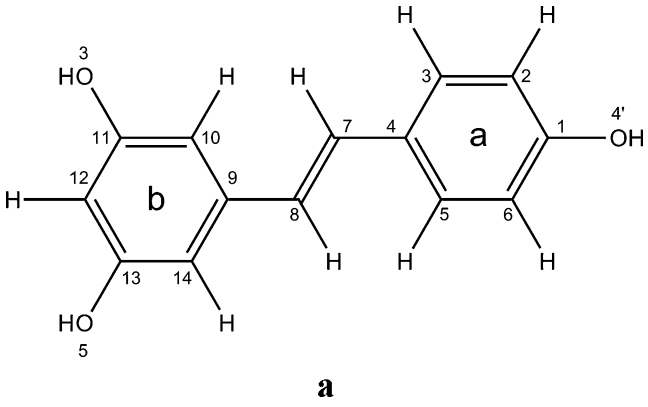

Fig. 1 Chemical structure of *trans*-resveratrol

suggested that this process can be associated with the chelation of Cu(II) by TR. Hence, the TR-Cu(II) complexes prevent the membranes of blood vessels from being affected by the harmful action of the peroxided LDL. Moreover, it has been shown that *cis*-stereoisomer of TR has significantly lower ability to chelate Cu(II).

To elucidate antiproliferative properties of TR and its analogues many experiments on cell and tissue cultures have been performed. Colin et al. [11] have shown effectiveness of TR and its triacetate derivative against human hepatoma cells (HepG2). Pozo-Guisado et al. [12] have studied the mechanism of the programmed cell death induction by TR in human breast cancer lines (MCF-7 and MDA-MB-231). Their results reveal that TR influences the regulation of the cell cycle and induces apoptosis in a concentration and cell-specific manner. Likewise, the studies of Roccaro et al. [13] on Waldenström's macroglobulinemia (WM) cells confirm inhibition of proliferation by TR and induction of cytotoxicity. In the study by Hsieh [14] it has been revealed that TR targets protein NQO2 - a mediator in modification of expression of NF-κB p65, which may contribute to the anti-prostate cancer activity of this polyphenol.

Recently, several studies have provided evidence that TR takes part in DNA-cleavage process. Kang et al. [15] have demonstrated that TR and its derivatives exert cytotoxic and proapoptotic activity in human promyelocytic leukaemia cells (HL-60). The compounds studied suppress cytochrome P-450 (CYP) 1B1 gene and induce the breakage of DNA strands which is consistent with apoptosis induction. Zhou et al. [16] have investigated the influence of TR on apoptosis of implanted primary gastric cancer cells in nude mice. The results demonstrated significant proapoptotic activity of TR on the implanted tumor cells and possible involvement of mediation of this process by apoptosis-regulated genes *bcl-2* and *bax*.

Understanding the role of TR in DNA damaging in cancer cells and explaining its antiproliferative and chemopreventive properties is very important and has prompted us to carry out a detailed quantum chemistry study of the interactions of TR with guanine-thymine dinucleotide (GpT) and DNA-derived nitrogenous bases (NB). Better knowledge of the structure, stability and structure-activity relations of these systems will undoubtedly help understand the therapeutic action of TR. In this paper, for the first time, intermolecular hydrogen bonding has been studied in TR-NB complexes. Moreover, we investigated physical properties of isolated components of the complexes considered using non-empirical *ab initio* methods which permit taking into account all contributions to the stabilization energy. The degree of agreement between MP2 data and DFT ones will give us insight into the nature of molecular interactions in the complexes investigated and will permit evaluation of the accuracy limits of these methods. Since water is the main component of all physiological fluids and living cells, the influence of aqueous solvation effects on the stability and geometrical parameters of the chemical systems presented has been investigated.

Computational details

In the present paper, all quantum-chemical computations were performed using Gaussian 03 computational package [17]. The geometries of chemical systems considered were fully optimized in their ground electronic state. Full optimization of each structure was performed without symmetry constraints. For each structure the force constants at the initial point of optimization were computed using the same methods and basis sets as for the optimization procedure. The geometries of GpT and TR-GpT (Fig. 2) systems were fully optimized employing Becke's three-parameter hybrid functional B3LYP with the gradient-corrected correlation functional by Lee, Yang and Parr [18] combined with the standard 6-311+G(d,p) basis set. The structures of TR-thymine (TR-T), TR-guanine (TR-G), TR-cytosine (TR-C) and TR-adenine (TR-A) complexes (Fig. 3) were fully optimized with the use of the restricted B3LYP/6-311G(d,p) level in vacuum and water medium, whereas isolated nitrogenous bases were fully optimized utilizing the MP2(full)/6-311G(d,p), MP2(full)/6-311+G(d,p), B3LYP/6-311G(d,p) and B3LYP/6-311+G(d,p) levels of theory. Finally, for the most stable geometries of TR-NB systems, the single-energy point calculations were performed to predict accurate values of total energy with the use of the MP2(full)/6-311G(d,p), MP2(full)/6-311+G(d,p) and B3LYP/6-311+G(d,p) levels, while for the most stable geometry of TR-GpT complex and isolated GpT more reliable energy was computed using the MP2(full)/6-311++G(3df,2p) and B3LYP/6-311++G(3df,2p) levels. All the energies discussed include zero-point effects. Employing the MP2 theory (with frozen core approximation) we

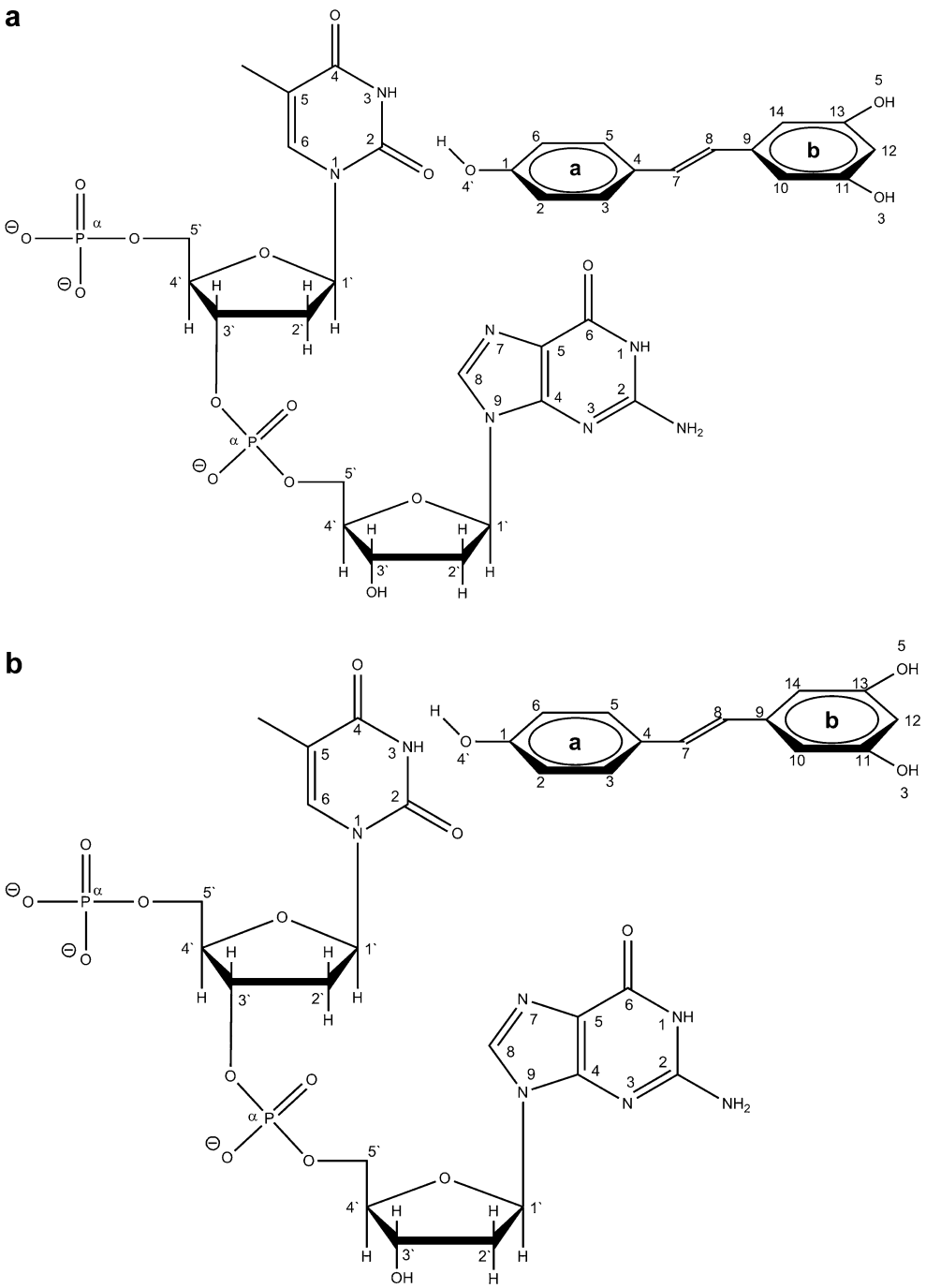

Fig. 2 **a-k** Structures of TR-4′-O-GpT system

evaluated the influence of electron correlation and dispersion effects on stabilization energies. MP2 single-point energy calculations and MP2 optimization of geometry and energy were performed with all electrons active. Since we employed very expensive MP2 method, only the interactions in simple TR-GpT complex were studied. Taking into regard that the contribution of the correlation energy to the total interaction energy of the complexes studied is very important, the MP2 (full) method was used. Furthermore, because the DFT method is deficient in proper description of dispersion attraction, the MP2(full) theory for the computations of stabilization energies was applied. Note that the dispersion energy component can contribute to stabilize the TR-GpT and TR-NB complexes and it is assumed to provide a high contribution to total stabilization energies of these systems. To determine the most energetically stable chemical systems we optimized geometries of several conformations of TR-GpT, TR-4′-O-T, TR-4′-O-G, TR-4′-O-C, TR-4′-O-A, TR-3-O-T,

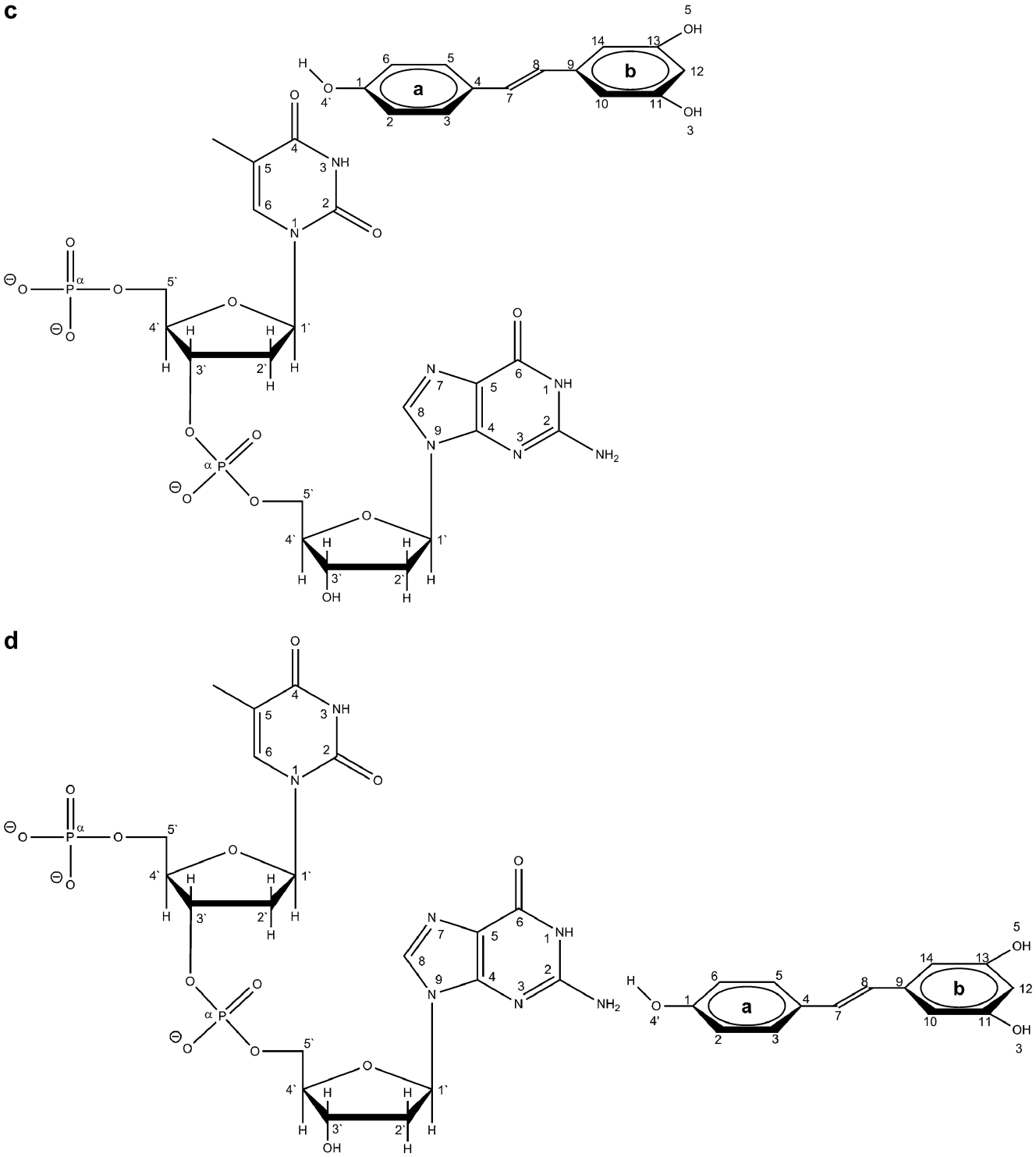

Fig. 2 (continued)

TR-3-O-G, TR-3-O-C and TR-3-O-A complexes (Figs. 2 and 3). Hence, computations were performed for all complexes corresponding to the positions known as the potential coordination place. The hydrogen bonds analysis between the atoms of 4′-OH and 3-OH groups of TR and donor atoms of NB was performed. In this way the abilities of these groups to form the H-bonds and their stabilities were compared. To assess the contribution of dispersion energy to the stabilization energy, the frequency-depended polarizabilities of TR and NB were

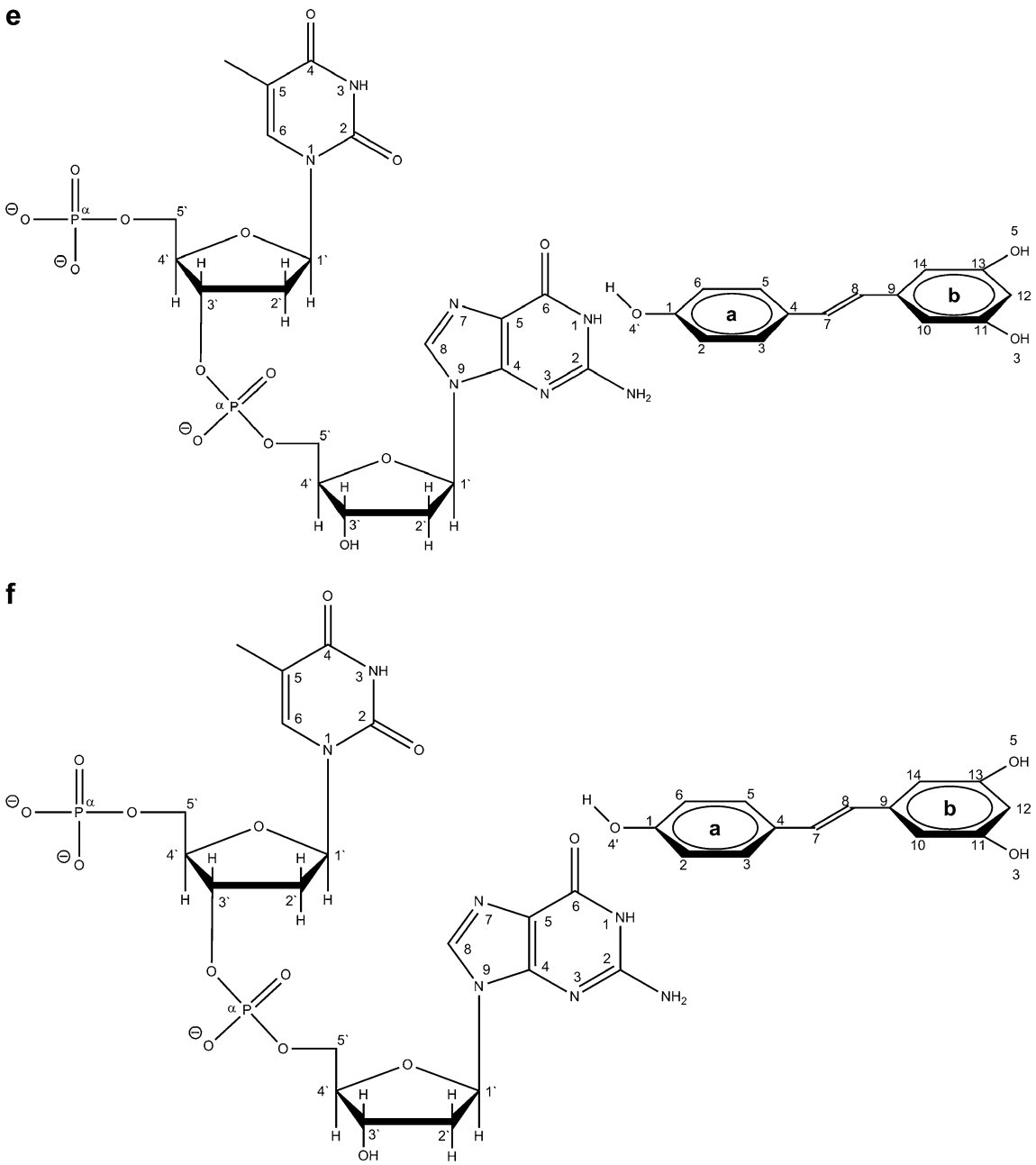

Fig. 2 (continued)

computed using ω=0.1. The dipole moment was computed as the first derivative of the energy, with respect to the applied electric field. This parameter is a measure of asymmetry in the molecular charge distribution.

In all computations we used dinucleotide with guanine and thymine fragments. Moreover, the monophosphate(V) groups in anionic form were applied in our calculations since such forms mainly occur in real biological systems. In particular, the total charge of TR-GpT complexes equal to -3 was applied. Hence, the multiplicity of these complexes equal to one was assumed. For neutral TR-NB complexes the multiplicity was equal to one. As in the phosphate group the protons are strongly acidic, these groups are negatively charged at pH near 7. We used basis sets with diffuse functions because TR-GpT complex was in anionic form. It is well known that the 3′-5′ phosphodiester bond assumes different conformations determined by the twist angles in the skeletons of deoxyribose. Hence, we studied the dinucleotide in which the carbon atom C2′ is in *endo* conformation with respect to C5′. Moreover, in this dinucleotide the nitrogenous bases are in *anti* conformation with respect to the N-glycosidic bond.

The potential energy surface (PES) scans (Supplementary materials) were made to determine the starting geometry of

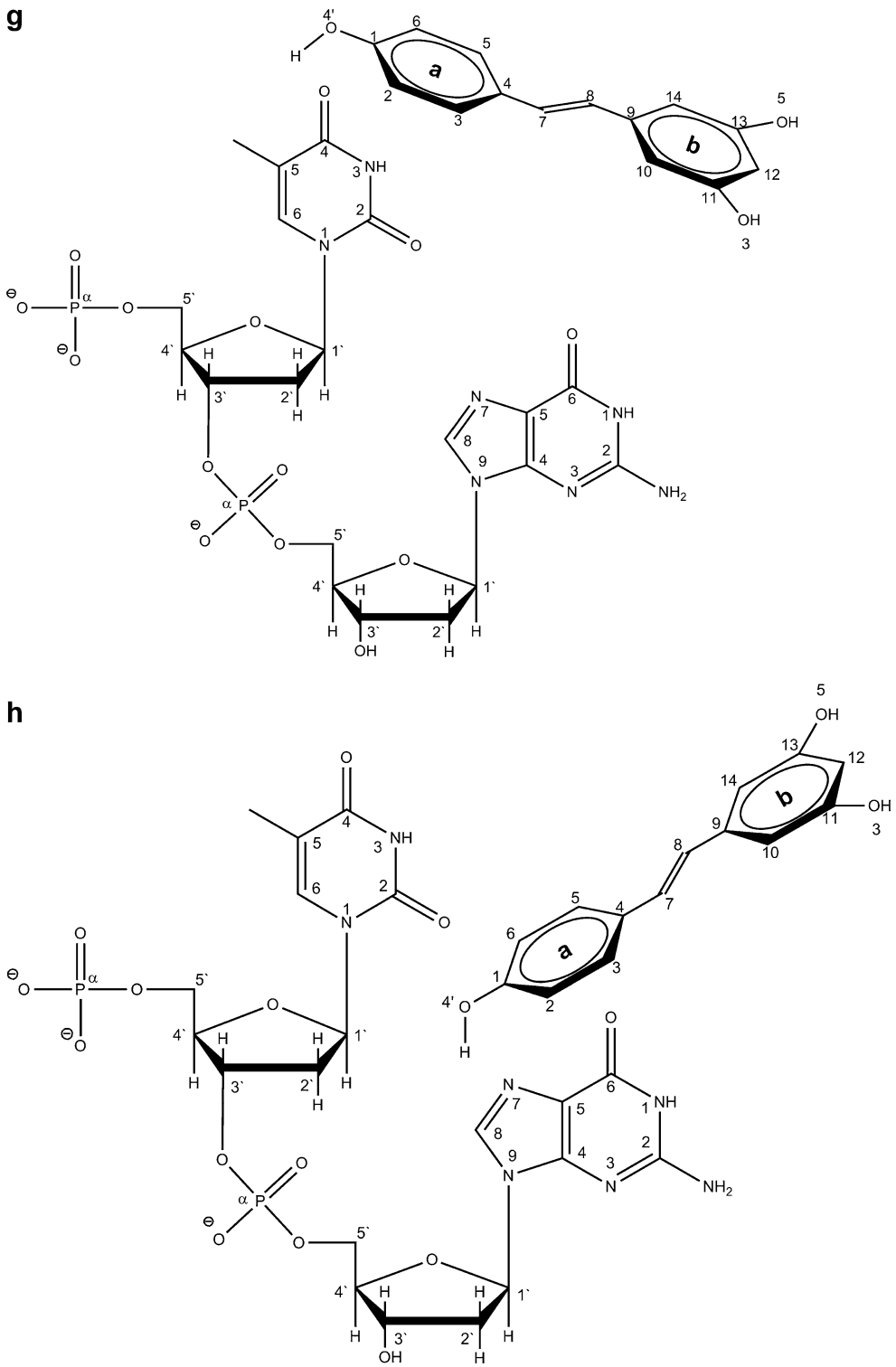

Fig. 2 (continued)

the chemical systems examined and the approximate location of the energy minimum structures. In particular, rotational potential profiles were obtained by scanning α (C5-C4-C7-C8) and θ (C7-C8-C9-C10) torsion angles of *trans*-stilbene skeleton of TR using the B3LYP/6-311G(d,p) and *ab initio* MP2(full)/3-21G levels of theory in vacuum. For TR-NB complexes PES were determined at the B3LYP/6-31G(d,p) level. These angles were scanned in steps of 10°, ranging from 0° to 180°. These PES allowed us to gather information about the orientation of the phenyl rings in relation to the vinyl bond and nitrogenous base skeleton. These surfaces were also generated at the B3LYP/6-311G

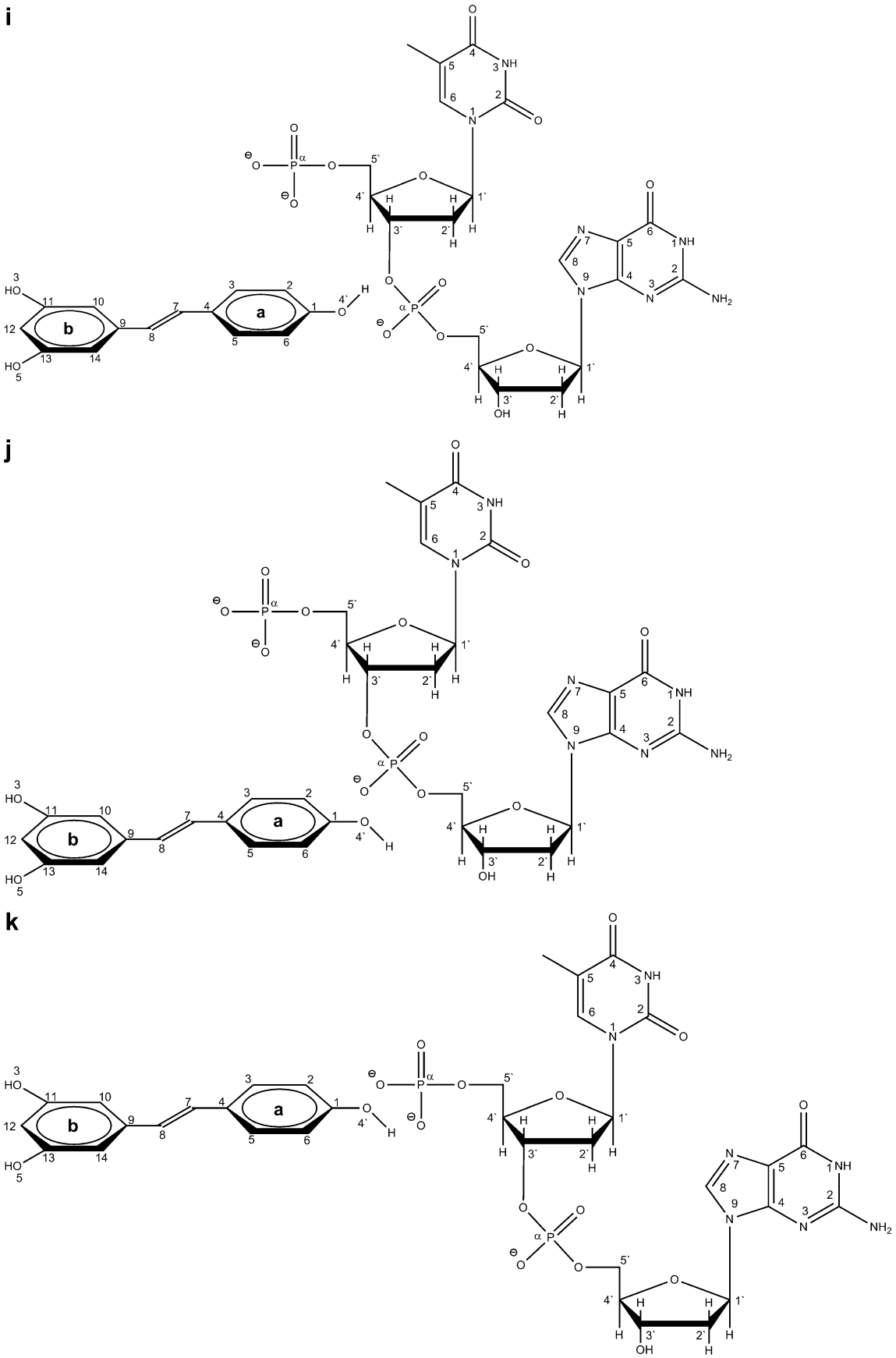

Fig. 2 (continued)

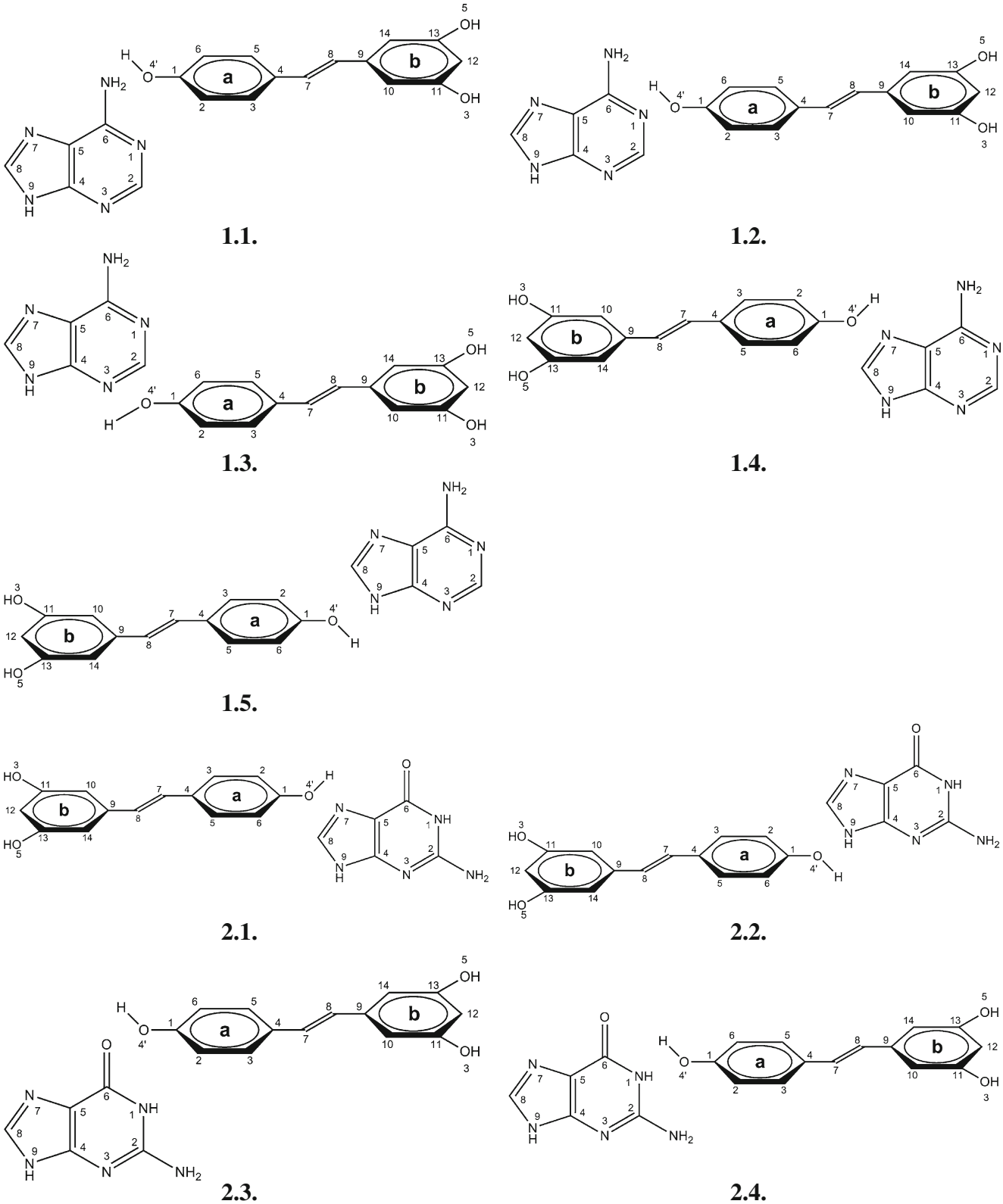

Fig. 3 Structures of TR-4′-O-NB complexes: 1) adenine, 2) guanine, 3) cytosine and 4) thymine

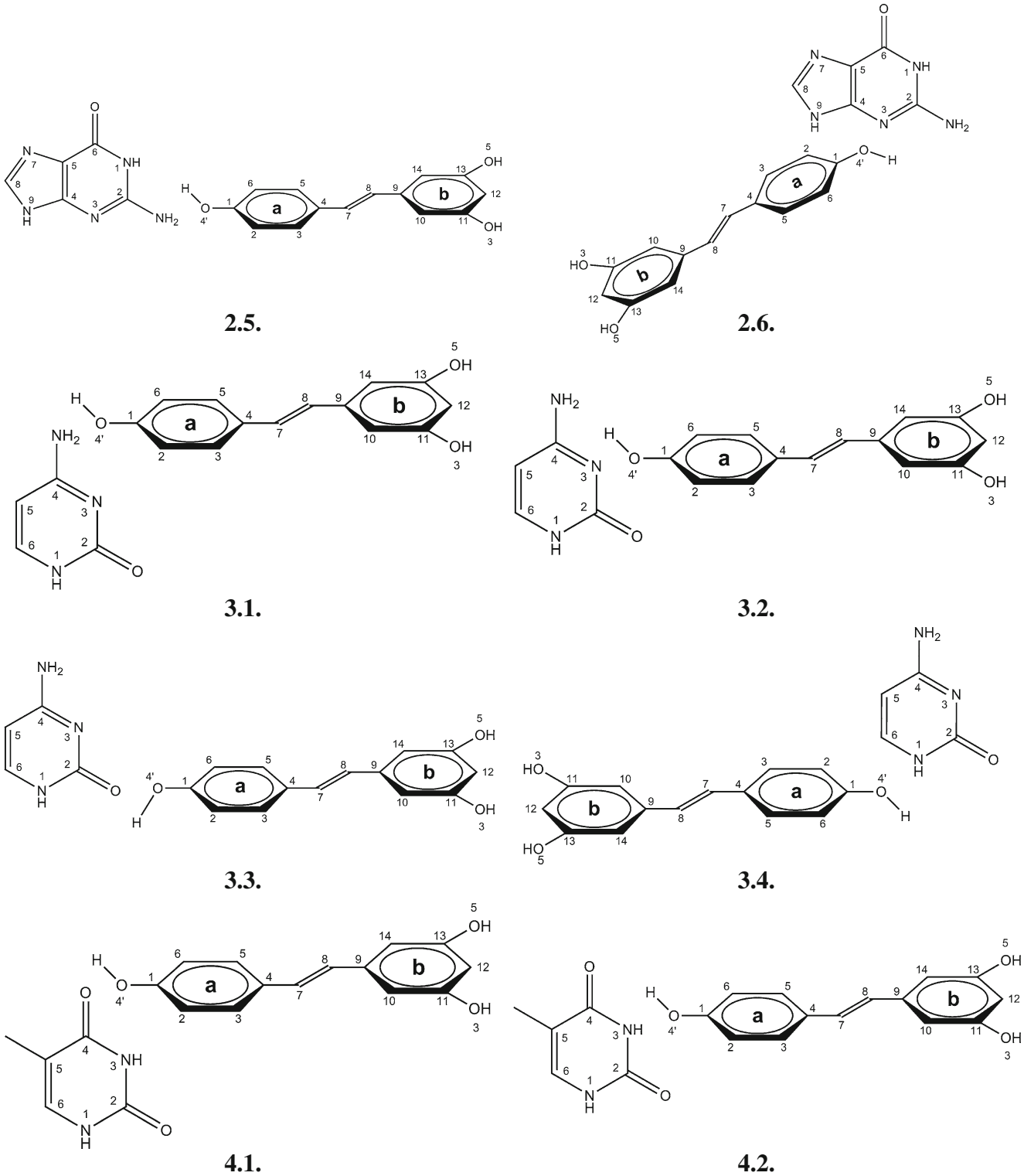

Fig. 3 (continued)

(d,p) and MP2(full)/6-311G(d,p) levels of theory by changing the torsion angles β (C6-C1-O4′-H4′), γ (C10-C11-O5-H5) and φ (C14-C13-O3-H3) of TR in 60° increments with constraint on all other geometrical parameters. The dihedral angles mentioned are fixed at each point of PES, while the other geometrical parameters are optimized. Afterwards, the selected lowest-energy structures obtained from the scan were fully optimized and vibrationally characterized without

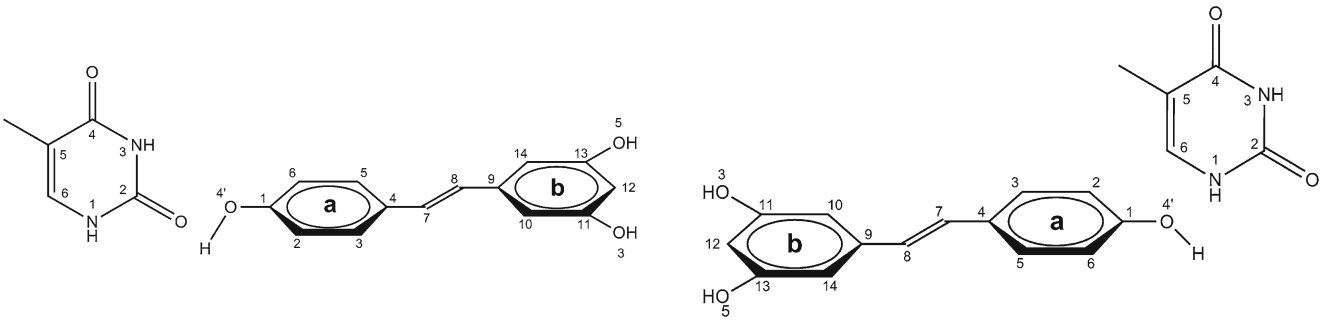

Fig. 3 (continued)

any constraints around each potential minimum. In this way, the most reliable structures of the complexes investigated and TR in the absolute energy minimum were determined.

The atomic charge distribution in TR was carried out with the use of natural bond orbital (NBO) population analysis at the B3LYP/6-311+G(d,p) level. For additional computations this charge distribution was obtained with the inclusion of electron correlation effects via the MP2(full)/6-311G(d,p) method. The geometry of TR was fully optimized at the B3LYP/6-311G(d,p), B3LYP/6-311+G(d,p), B3LYP/6-311++G(3df,2p) MP2(full)/6-311G(d,p), MP2(full)/6-311+G(d,p) and MP2(full)/6-311++G(3df,2p) levels. For all fully optimized structures, the harmonic vibrational frequencies and zero point energy corrections were computed analytically and scaled by the factor of 0.973 as recommended. We calculated the harmonic vibrational frequencies of the corresponding bonds to determine stationary points on PES. The nature of the stationary points was characterized by analyzing the number of imaginary frequencies: 0 corresponded to a minimum and 1 corresponded to a saddle point (transition state). These frequencies were obtained from analytical diagonalization of the corresponding Hessian matrices.

The stabilization energies ΔE_{stab} (without deformation and sterically corrected stabilization) were computed as the differences in the electronic energies of the complex systems and the energies of the isolated chemical systems (TR, GpT and NB). Hence, the stabilization energies were computed adopting the following formula proposed by Pavelka et al. [19]:

$$\Delta E_{stab} = -\left(E_{complex} - \sum_{i}^{monomers} (i)\right) \quad (1)$$

where $E_{monomer}$ is the electronic energy of the fully optimized geometry of individual subsystem (Tables 1, 2 and 3), while $E_{complex}$ is the electronic energy of the whole complex studied (Tables 1, 2 and 3). The deformation energies were not computed because the complexes studied do not contain ligand shell around metal cation. In the case of complexes containing ligands and metal cation, the ligands are considered as one monomer and metal cation as another one [20]. In this way the sterically corrected stabilization energy can be computed. Note that these stabilization energies permit evaluation of stability of the complexes investigated. The high value of this energy is correlated with high energetic stability. To investigate the relative stability of the complexes considered more carefully, we assessed the basis set superposition error (BSSE) by counterpoise correction (CP) [21]. The CP approach systematically removes the basis superposition errors. In this way we obtained more accurate values of the counterpoise-corrected stabilization energies. The stabilization energies for the most stable geometries of the TR-4′-O-NB systems were computed at the B3LYP/6-311G(d,p), B3LYP/6-311+G(d,p), MP2(full)/6-311G(d,p) and MP2(full)/6-311+G(d,p) levels, whereas for the TR-GpT system at the B3LYP/6-311++G(3df,2p) and

Table 1 The computed total energies E_{total} [hartree] for TR, nitrogenous bases and TR-4′-O-NB and TR-3-O-NB complexes at the B3LYP/6-311G(d,p) level

Compound	E_{total} (vacuum)	E_{total} (water medium)
TR	-766.57104560	-766.61348512
Adenine	-467.43921416	-467.4668243
Guanine	-542.69791707	-542.74216496
Cytosine	-395.04103019	-395.07657077
Thymine	-454.26287272	-454.29255507
TR-4′-O-A	-1234.03154807	-1234.08740995
TR-4′-O-G	-1309.28994513	-1309.36384876
TR-4′-O-C	-1161.63721636	-1161.69740573
TR-4′-O-T	-1220.85400531	-1220.90658855
TR-3-O-A	-1234.03169814	-1234.08746209
TR-3-O-G	-1309.36188089	-1309.41211008
TR-3-O-C	-1161.69711258	-1161.75325659
TR-3-O-T	-1220.91198033	-1221.17654306

Table 2 The computed total energies (E_{total}) [hartree] of TR, nitrogenous bases and TR-4′-O-NB complexes in vacuum at the B3LYP/6-311+G(d,p), MP2(full)/6-311G(d,p) and MP2(full)/6-311+G(d,p) levels

Compound	E_{total} B3LYP/ 6-311 + G(d,p)	E_{total} MP2(full)/ 6-311G(d,p)	E_{total} MP2(full)/ 6-311 + G(d,p)
TR	-766.58913303	-764.39630849	-764.42594973
Adenine	-467.45139235	-466.4300479	-466.36253436
Guanine	-542.71281002	-541.45006976	-541.47639141
Cytosine	-395.05306396	-394.10811392	-394.12798926
Thymine	-454.27359263	-453.20149699	-453.22314693
TR-4′-O-A	-1234.05685118	-1230.56737707	-1230.61765931
TR-4′-O-G	-1309.31918536	-1306.18834028	-1306.24602476
TR-4′-O-C	-1161.66193183	-1158.337708184	-1158.42466528
TR-4′-O-T	-1220.87822469	-1217.93960087	-1217.98946243

MP2(full)/6-311++G(3df,2p) methods. To compare the stability of the TR-4′-O-NB and TR-3-O-NB complexes for the TR-3-O-NB systems the stabilization energies were estimated at the B3LYP/6-311G(d,p) level. The PDE (*Proton dissociation enthalpy*) value of the 4′O-H bond in TR was computed at the B3LYP/6-311+G(d,p) level according to the equation: $PDE = H_{anion} + H_{proton} - H_{molecule}$ in which, H_{anion} is the enthalpy of the 4′-O-anion generated after proton abstraction, H_{proton} is the enthalpy of proton while $H_{molecule}$ stands for the enthalpy of the parent molecule TR. The enthalpy of the proton in vacuum is given by its translation energy, $H[H^+(g)] = 3/2\ kT$ [22].

The aqueous effects were determined using the conductor-like polarizable continuum solvation model (C-PCM) [23] implemented in the Gaussian 03 program. In this model water is assumed as a macroscopic continuum characterized by the dielectric constant ε=78.39. The UAO model of solvation radii was used in the computations to build the cavity. The UAO cavity is built up using the united atom topological model UATM [24] applied to atomic radii of the universal force field UFF. The C-PCM computations were performed with tesserae of 0.2 $Å^2$ average size. The solvent effect in the conformational equilibrium was obtained for the optimized most stable chemical systems studied in the vacuum. We investigated the influence of the solvent effects on the ΔE_{stab} values because several chemical systems examined are charged species and thus are able to strongly interact with polar environment.

Table 3 The computed total energies (E_{total}) [hartree] of TR, nitrogenous bases and TR-4′-O-NB complexes in water medium at the B3LYP/6-311+G(d,p), MP2(full)/6-311G(d,p) and MP2(full)/6-311+G(d,p) levels

Compound	E_{total} B3LYP/ 6-311 + G(d,p)	E_{total} MP2(full)/ 6-311G(d,p)	E_{total} MP2(full)/ 6-311 + G(d,p)
TR	-766.63298106	-764.4371911	-764.47143274
Adenine	-467.48035934	-466.36748194	-466.67942532
Guanine	-542.76037976	-541.49219699	-541.52212558
Cytosine	-395.09193251	-394.14190468	-394.16549561
Thymine	-542.76037976	-453.22941540	-453.2518931
TR-4′-O-A	-1234.11359319	-1230.62117861	-1230.67463010
TR-4′-O-G	-1309.39265554	-1306.25732004	-1306.31851650
TR-4′-O-C	-1161.72117079	-1158.43212940	-1158.96002614
TR-4′-O-T	-1220.93369400	-1217.99015509	-1218.04357626

Results and discussion

Conformational and energetic analysis for the TR-GpT complexes

From all the structures presented in Fig. 2 the lowest energy conformation is **2i**. The equilibrium values of energies computed at the B3LYP/6-311+G(d,p) level (Table 4) support this conclusion. A close look at the most stable fully optimized structure of TR-GpT (Fig. 4) reveals that TR has strictly planar and semi-quinone geometry. This geometry was found as an absolute minimum on the PES. The strong interaction of this polyphenol with negatively charged oxygen atoms of the 3′-5′ phosphodiester bond mainly contributes to generate this unique geometry of TR which can be strongly stabilized by resonance. Hence, this resonance stabilization can be mainly responsible for high stability of the complexes studied. Summarizing, this result proves the TR-GpT interaction considered serves to facilitate the activation of this semi-quinone structure of TR. In the system **2i** the optimized value of the distance between 4′-H and 4′-O atoms is 1.606 Å, while in the isolated TR molecule the 4′-O-H bond length is 0.967 Å. However, the optimized distance between 4′-O atom of TR and phosphorus atom is 4.553 Å. We observe that the proton from the 4′-OH group migrates to the 3′-O atom of dinucleotide since in the equilibrium geometry (Fig. 4) the 4′-H atom is bonded with the 3′-O atom of the dinucleotide. The optimized value of the 3′O-4′H formed bond is 0.992 Å, which confirms that this bond is stable. These findings lead to the conclusion that during the interaction of TR with GpT, TR functions as the proton donor, while 3′-O atom of dinucleotide is the acceptor of this proton. The value of PDE computed at the B3LYP/6-311+G(d,p) level for the 4′-O-H bond in isolated molecule of TR is 322.58 kcal mol^{-1}, whereas in water medium PDE is 281.16 kcal mol^{-1} [22]. This result proves that the interaction of the 4′O-H bond with strongly nucleophilic phosphoric group and polar medium can lead to breaking this bond. Consequently, the proton can easily migrate form the 4′-OH group to the 3′-O atom of dinucleotide in water medium. These findings suggest that the polarization effects and the strong Coulomb interaction

Table 4 The computed stabilization energies ΔE_{stab} [kcal mol^{-1}] and ΔE_{stab}+BSSE [kcal mol^{-1}] of TR-GpT complexes at the B3LYP/6-311++G(3df,2p) level as well as total energies [hartree] at the B3LYP/6-311+G(d,p) level

Complex	Energy	ΔE_{stab} (vacuum)	ΔE_{stab} + BSSE (vacuum)	ΔE_{stab} (water medium)	ΔE_{stab} + BSSE (water medium)
2a	-3363.3125236	93.23	92.12	136.32	135.02
2b	-3363.3179202	96.41	95.03	139.43	138.40
2c	-3363.3198801	95.53	94.42	138.54	137.81
2d	-3363.3078342	96.23	95.43	139.20	138.23
2e	-3363.3026434	90.74	89.74	131.76	130.01
2f	-3363.3069125	92.43	91.78	132.79	130.93
2g	-3363.3082319	93.15	91.98	133.03	131.87
2h	-3363.3030595	93.15	91.89	133.59	131.79
2i	-3663.3227366	100.67	98.23	142.85	140.04
2j	-3663.3212454	98.45	98.53	141.35	139.73
2k	-3663.3215778	97.98	96.04	139.56	138.30

of TR with negatively charged oxygen atoms of dinucleotide lead to a decrease in the strength of the 4′O-H bond of TR. Heterolytic dissociation of 4′O-H bond can be a consequence of this interaction. Moreover, a more significant role in breaking of the 4′O-H bond is played by donation from oxygen of P-O bond into the empty 4′-OH orbital. The partial charge computed at the B3LYP/6-311+G(d,p) level on 4′-O atom in isolated molecule of TR is -0.359, whereas in **2i** complex it is -0.468. This result supports the conclusion that in **2i** complex 4′-O-H bond breaks and in consequence forms the anionic form of TR. In order to get more detailed insight into the origin of 4′O-H bond breaking, molecular orbital analysis related to 4′O-H-O-P bonding will be performed in the future. It is interesting to note that in the presence of TR the distance between O3′ atom and P atom is 2.955 Å, while in the optimized geometry of GpT this distance is equal to 1.69 Å. These values in water medium are smaller and equal to 2.821 Å and 1.523 Å, respectively. It is probably due to higher stabilization of the system by water. This very high value of the O3′-P bond length in TR-GpT complex indicates that the 3′-5′ phosphodiester bond breaks in the presence of this compound. Note that the transfer of the proton from 4′-OH group of TR to 3′-O atom of dinucleotide in water medium can lead to breaking the 3′-5′ phosphodiester bond. It should be stressed that each phosphodiester bond in DNA strand has negative charge, hence it is weakly susceptible to hydrolysis. Hydrolysis of this bond can be catalyzed by phosphodiesterases and bacterial restriction endonucleases which play a crucial role in repairing DNA sequences. However, our result demonstrates that TR apart from various hydrolytic agents can induce the DNA strand cleavage. On the basis of the fact that DNA cleavage is one of the most important steps of the degradation of cancer cells we theoretically confirmed that this compound has a potent anticancer and antiproliferative influences on tumors growth. This result confirms the experimental observation reported in the study by Kang et al. [15]. The results obtained suggest that TR attacks monophosphate(V) group and in consequence covalent and 5-coordinated transition product can form. At the second step the 3′-5′ phosphodiester bond breaks in this

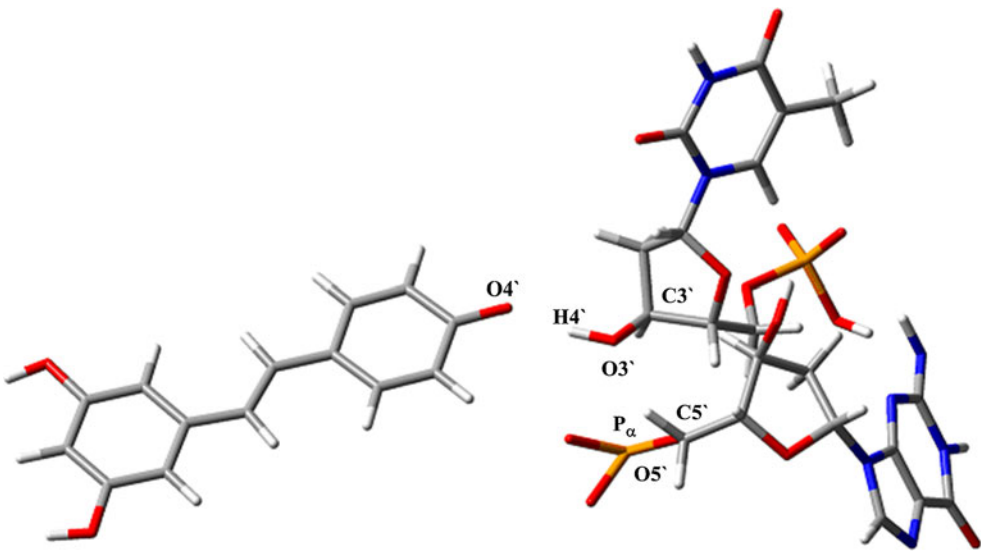

Fig. 4 Fully optimized geometry of TR-GpT complex at the B3LYP/6-311G(d,p) level in vacuum

unstable product. Investigation of the mechanism of the interaction of TR with dinucleotide proposed and the reaction path analysis are in progress.

It is well known that DNA topoisomerase I (topI) is an enzyme which is a cellular target for many anticancer and antiproliferative drugs. This essential enzyme induces reversible cleavage of single- and double-stranded DNA in cells [25]. Several theoretical studies have proved that the presence of covalent topoisomerase I-DNA-inhibitor ternary complex stabilized by hydrogen bond effectively blocks relegation and enzyme release leading to permanent DNA strand cleavage [26]. Also, it has been shown that TR is able to interact with this enzyme in cancer cells. Hence, our results suggest that *trans*-resveratrol can be an inhibitor of topoisomerase I inducing topI-DNA breaks by preventing DNA relegation. This suggestion is mainly supported by the fact that cleavable TR-GpT complex is characterized by high stability. To verify this hypothesis further investigation of the geometry and stability of topI-DNA-TR complex should be undertaken.

The fully optimized values of bond lengths in the TR-GpT complexes (Table 5) indicate that the hydrogen bond between 4′-H of TR and carbonyl-oxygen atoms is more stable than the ones between 4′-H, nitrogen imidazole and amine atoms of guanine and thymine fragments. In particular, the length of the hydrogen bonds between 4′-H atom and carbonyl O(2), O(4) and O(6) atoms of thymine and guanine residue are approximately 1.45 Å. It proves that these bonds are particularly stable. This result suggests that TR can interact with GpT also by formation of the stable hydrogen bonds with nitrogenous bases. In real biological systems the interaction of TR with DNA strand can be affected by factors such as water which strongly interacts with anionic forms of dinucleotide. Hence, our theoretical approach with the solvation model is more reliable.

The high values of the computed stabilization energies (Table 4) prove that all complexes studied show high stability and that components of complex Fig. 2i are the strongest bonded. These results demonstrate that the ability of this polyphenol to bind with the DNA strand and its monophosphate(V) group can be especially preferable in real biological systems. The computations on the MP2(full)/6-311++G(3df,2p) level (Table 6) demonstrate that the values of the stabilization energies increase in comparison with the results obtained on the B3LYP/6-311++G(3df,2p) level (Table 4). It strongly proves that the electron correlation effects should be included in the computations to accurately describe the binding interactions in the complexes considered. Note that, the dispersion attraction, which is part of the π-π interactions between planar skeletons of TR and nitrogenous bases in TR-GpT complexes, is included in the MP2 values of ΔE_{stab}. On the basis of ΔE_{stab} obtained at the MP2(full)/6-311++G(3df,2p) we can conclude that dispersion term represents non-negligible contribution to high stability of TR-GpT complexes. Since dinucleotide is a negatively charged system, the electrostatic ion-dipole and dipole-dipole contributions as well as attractive induction term to total stabilization energies obtained at the B3LYP/6-311G(3df,2p) level are significant. When the solvent effect was taken into account a substantial influence of water medium on the ΔE_{stab} values was noticed. The values of this stability factor in water medium are dramatically higher than in vacuum because the charged systems studied are very sensitive to the polarity of water environment. This finding clearly indicates that water environment strongly contributes to enhance the stability of TR-GpT systems.

Table 5 The optimized values of the selected hydrogen bond lengths [Å] of TR-GpT complexes (Fig. 2) obtained at the B3LYP/6-311+G(d,p) level. These values are referred to vacuum

Bond	Bond length
H4′-O(2)	1.452
H4′-N(3)	1.823
H4′-O(4)	1.454
H4′-N(2)	2.134
H4′-N(1)	1.827
H4′-O(6)	1.455
H4′-N(7)	1.881

Interactions between TR and nitrogenous bases. Hydrogen bonds analysis

The fully optimized geometries of the TR-NB complexes are presented in Fig. 5. These structures represent absolute energy minimum on PES. The computed values of total energies of these complex systems are referred to global energy minimum obtained on the PES (Tables 1, 2 and 3).

Table 6 The computed stabilization energies ΔE_{stab} [kcal mol^{-1}] and ΔE_{stab} + BSSE [kcal mol^{-1}] of TR-GpT complexes at the MP2(full)/6-311++G(3df,2p) level

Complex	ΔE_{stab} (vacuum)	ΔE_{stab} + BSSE (vacuum)	ΔE_{stab} (water medium)	ΔE_{stab} + BSSE (water medium)
2a	99.48	98.21	142.54	141.23
2b	100.34	98.78	143.75	142.54
2c	101.45	100.03	144.09	143.64
2d	102.49	101.34	145.89	144.01
2e	97.56	96.60	138.86	137.12
2f	98.02	97.54	139.87	138.42
2g	99.56	98.04	140.76	139.10
2h	99.86	98.54	140.99	139.76
2i	110.30	108.95	147.96	146.54
2j	107.89	106.21	145.53	143.45
2k	105.56	104.31	144.01	142.87

In these systems TR is characterized by strictly planar geometry of *trans*-stilbene skeleton. Furthermore, in the fully optimized structure of the TR-G complex the planar skeletons of guanine and TR lie in the same plane, while OH groups of TR lie in plane of *trans*-stilbene skeleton. The analysis of the relative energetic stability (Table 1) of the TR-3-O-NB and TR-4′-O-NB (Fig. 5) complexes reveals that the TR-3-O-G, TR-3-O-C and TR-3-O-T systems are signif-

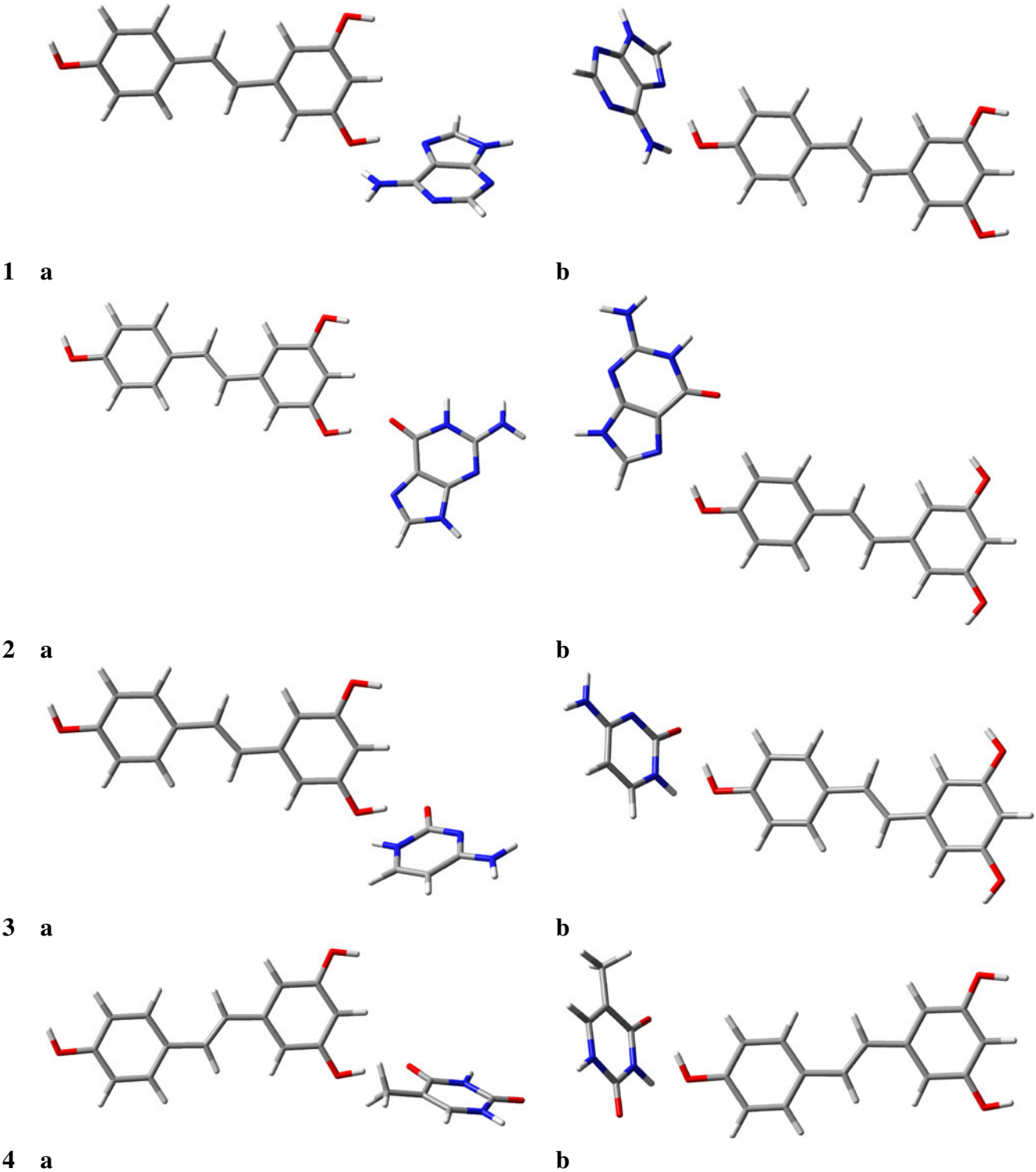

Fig. 5 Geometries of selected TR-3-O-NB (**a**) and TR-4′-O-NB (**b**) complexes: 1) adenine, 2) guanine, 3) cytosine and 4) thymine fully optimized at the B3LYP/6-311G(d,p) level in vacuum

icantly more stable in the media considered than TR-4′-O-G, TR-4′-O-C, TR-4′O-T ones. However, the TR-4′-O-A and TR-3-O-A complexes show comparable stability in the media studied. Short lengths of hydrogen bonds in these structures (Table 7) are an interesting feature of these systems. In particular, H-bonds usually have lengths from the range 1.708-2.041 Å in vacuum, while in water medium this range is 1.672-2.129 Å. Therefore, in the presence of polar medium the H4′-N(7), H4′-O(2) and H4′-O(4) H-bonds formed are stronger than in vacuum. This result suggests that in the water environment of the cells, TR mainly bonds with NB through hydrogen bonds. Note that the 4′H-N(amine) H-bond in TR-A complex is more stable in vacuum than in water medium. In the TR-A and TR-G complexes the H-bond between 4′-H atom of TR and nitrogen imidazole atom of adenine and guanine are stable. Possible explanation of this fact is a rather high donation of nitrogen imidazole atom. It should be stressed that the TR-T complex exhibits the shortest H4′-O(2) and H4′-O(4) bonds in water medium, while TR-C system is characterized by the shortest H4′-O(2) bond in this medium (Table 7). Hence, these bonds mainly contribute to enhancement of energetic stability of TR-C and TR-T systems. Analogous effects are also noticeable in TR-C and TR-T systems, in which strong H-bonds are formed by 4′-H atom of TR and carbonyl oxygen atom of cytosine and thymine. The values of these H-bonds lengths reveal that they are stronger than H-bonds in TR-A and TR-G systems. As follows from analysis of the H-bonds formed by the 4′-OH and 3-OH groups of TR, the stability of these bonds is very similar. Practically identical distances between the 4′-H and 3-H atoms and the donor atoms of NB confirm this observation. This result suggests that in biological systems 4′-OH and 3-OH groups participate in formation of stable H-bonds with DNA nucleobases.

Tables 8 and 9 present one-electron properties (dipole moment and polarizability) of TR and NB in the media studied. From these results we find that TR has very large polarizability at the DFT and MP2 methods. The polarizabilities obtained at the restricted B3LYP/6-311G(d,p) level for nucleobases are in satisfactory agreement with those obtained by Riahi et al. [27]. This fact supports the conclusion that dispersion energy should bring high contribution to the interaction energy of the complex studied. Moreover, all interacting systems are characterized by higher values of polarizability in water medium than in vacuum (Table 9). From this result, it becomes clear that in water dispersion energy predominantly contributes to stability of the TR-NB complexes.

After geometry optimization, the stabilization energies in vacuum and water medium for TR-4′-O-NB systems were computed at the DFT level. In Table 10 uncorrected stabilization energies and stabilization energies with BSSE correction for these systems are collected. The obtained values of this energy clearly prove that the components of the binary systems studied are strongly bonded in vacuum. Probably, as a result of the presence of strong H-bonds these complexes show high stability. The stabilization energies computed at the DFT level reveal that the TR-C complex is the most stable in vacuum. In our opinion the values of ΔE_{stab} reflect the dominant role of many factors (for example, Coulomb attraction contribution) to the total stabilization energies. The work, in which the dominant contribution to ΔE_{stab} will be determined is in progress. The higher B3LYP/6-311G(d,p) and B3LYP/6-13+G(d,p) values of ΔE_{stab} of the TR-4′-O-C complex have been obtained in comparison with the ΔE_{stab} of the other systems (Table 10). This result suggests that in the TR-4′-O-C complex not only electrostatic interactions but also polarization energy and covalent bonding with higher donation have to play an important role in vacuum. The values of ΔE_{stab} obtained at the B3LYP/6-311G(d,p) level for the TR-4′-O-T and TR-3-O-T (Tables 10 and 11) complexes show opposite trend of stability in water medium. In this medium TR-3-O-T system reveals significantly higher stability than TR-4′-O-T complex. TR-3-O-A and TR-3-O-G complexes are slightly more stable than TR-4′-O-A and TR-4′-O-G ones. Therefore, this result demonstrates that both the 4′-OH and 3-OH group have similar abilities to bind NB, which is in good agreement with the H-bond analysis performed above.

The finding obtained at the MP2(full)/6-311+G(d,p) method indicates that water environment strongly contributes

Table 7 The optimized values of the selected hydrogen bond lengths [Å] of TR-4′-O-NB complexes at the B3LYP/6-311G(d,p) level. These values are referred to vacuum

Bond Type	TR-Adenine		TR-Guanine		TR-Cytosine		TR-Thymine	
	vacuum	water medium	vacuum	water medium	vacuum	water medium	vacuum	water medium
H4′-O(2)	-	-	-	-	1.708	1.665	1.799	1.748
H4′-O(4)	-	-	-	-	-	-	1.797	1.746
H4′-N(NH_2)	2.041	2.129	2.033	2.115	-	-	-	-
H4′-N(7)	1.810	1.753	1.880	1.777	-	-	-	-

Table 8 The computed values of dipole momentum (μ) [D] and polarizability (α) [Å^3] for TR and nitrogenous bases at the B3LYP/6-311G(d,p) and MP2(full)/ 6-311G(d,p) levels in vacuum

Parameter	B3LYP/6-311G(d,p)					MP2(full)/ 6-311G(d,p)				
	TR	A	G	C	T	TR	A	G	C	T
μ	2.108	2.379	6.518	6.392	4.233	3.597	2.520	6.928	7.258	4.864
α	166.32	112.99	124.76	93.370	98.40	169.46	109.72	126.63	94.35	96.90

to the increase in the stability of TR-4′-O-C complex (Table 10). Note that in water medium this complex is significantly more stable than in vacuum. However, the results obtained at the B3LYP/6-311G(d,p) and B3LYP/6-311+G(d,p) levels prove that water environment strongly contributes to reduction of the stability of TR-T complexes (Tables 10 and 11). This fact suggests that in water medium the strong repulsive electrostatic interaction of the complexes with water medium is more dominant than in vacuum and consequently, the components of the TR-T complex are not as strongly bonded in polar medium as in vacuum. It should be noted that despite this fact all TR-NB complexes are characterized by lower energy in water medium than in vacuum (Tables 1, 2 and 3). Probably strong repulsive interactions in water medium substantially dominate over the stabilizing interactions caused by strong hydrogen bonds. Hence, the solvation effects play an important role in reduction of stability of neutral TR-NB complexes. It could be argued that a decrease in stability in polar medium at the MP2 level can be attributed to dominance of dispersion repulsion over attractive interactions.

The computations performed with the use of the MP2 level demonstrate that the TR-A and TR-C complexes are significantly less stable than at the DFT level in the media considered (Tables 2 and 3) and that strong repulsion between components of these complexes mainly contributes to small stability. It suggests that at the correlated method the dispersion repulsion which corresponds to the van der Waals interaction contributes to reduce stabilization of the complexes studied. Also, the long-range exchange repulsions can cause the decrease in stability of these complexes. On the other hand, we conclude that the electron correlation leads to a small correction to the Coulomb term due to low polarity of the interacting monomers. However, TR-G and TR-T systems are significantly more stable at the MP2 level than at the DFT one. This result proves that in TR-G and TR-T complexes strong dispersion attraction can bring a dominant stabilization contribution. Hence, the correlated MP2 method, which is extended to cover the London attractive interactions, yields satisfactory stabilization energies for TR-G and TR-T complexes. Since DFT method basically ignores dispersion attraction [28], to obtain more reliable values of ΔE_{stab} a recently introduced method should be used in the future. This method is based on a combination of the approximate tight-binding DFTB with empirical dispersion energy. Also, the XB3LYP functional [29], which yields an accurate dispersion energy is needed to improve DFT results. The presence of flat and aromatic rings in TR and NB seems to be an important factor responsible for weak π-π interactions. This non-covalent interaction is mainly caused by intermolecular overlapping of p-orbitals of π-conjugated system of TR and NB which have strongly delocalized π-electrons. In addition, the π-π interactions consist of the London dispersion forces that arise from the forces between instantaneous multipole moments of the subsystems considered. In our opinion π-electronic structure of the compounds studied and their geometrical properties are mainly responsible for the contribution of the London dispersion energy to the computed stabilization energies. The negative values of ΔE_{stab} obtained at the MP2(full)/6-311G(d,p) and MP2(full)/6-311+G(d,p) for the TR-4′-O-A and TR-4′-O-C complexes as well as at the B3LYP/6-311+G(d,p) level in water medium for TR-4′-O-G, TR-4′-O-C and TR-4′-O-T systems (Table 10) suggest that strong electrostatic repulsion between components of these complexes significantly dominates over attractive interactions. Moreover, the negative values of the ΔE_{stab} obtained at the MP2 level (Table 10) prove that the electron correlation effects lead to dramatic decrease in stability, which is probably due to a reduction of the polarity of TR-4′-O-A and TR-4′-O-C complexes.

The difference between B3LYP/6-311+G(d,p) and B3LYP/6-311G(d,p) stabilization energy in the media studied was found (Table 10). The presence of the diffuse functions in the basis sets can decrease the energy values and accordingly the stability of the systems studied. However, the opposite trend is observed at the MP2 level for the TR-A, TR-C and TR-G complexes.

Table 9 The computed values of dipole momentum (μ) [D] and polarizability (α) [Å^3] for TR and nitrogenous bases at the B3LYP/6-311G(d,p) in water medium

Parameter	TR	A	G	C	T
μ	2.976	3.463	9.673	9.341	5.881
α	198.45	156.99	167.39	129.07	129.14

Table 10 The computed stabilization energies ΔE_{stab} [kcal mol^{-1}] and ΔE_{stab} + BSSE [kcal mol^{-1}] for the most stable geometries of TR-4′-O-NB complexes

Method	ΔE_{stab} (vacuum)	ΔE_{stab} + BSSE (vacuum)	ΔE_{stab} (water medium)	ΔE_{stab} + BSSE (water medium)
TR-4′-O-Adenine				
B3LYP/6-311G(d,p)	13.36	12.34	4.54	2.73
B3LYP/6-311+G(d,p)	10.24	9.12	0.16	0.11
MP2(full)/6-311G(d,p)	-93.05	-91.04	-115.14	-112.10
MP2(full)/6-311+G(d,p)	-107.19	-104.23	-298.84	-296.24
TR-4′-O-Guanine				
B3LYP/6-311G(d,p)	13.17	12.03	5.14	3.31
B3LYP/6-311+G(d,p)	10.31	8.75	-0.44	-0.15
MP2(full)/6-311G(d,p)	214.58	211.23	205.78	202.83
MP2(full)/6-311+G(d,p)	215.66	213.88	203.91	201.24
TR-4′-O-Cytosine				
B3LYP/6-311G(d,p)	15.78	14.32	4.61	2.15
B3LYP/6-311+G(d,p)	12.38	10.43	-2.35	-1.02
MP2(full)/6-311G(d,p)	-79.91	-76.98	-92.22	-89.11
MP2(full)/6-311+G(d,p)	-81.12	-78.23	202.75	198.46
TR-4′-O-Thymine				
B3LYP/6-311G(d,p)	12.60	10.87	-0.34	-0.12
B3LYP/6-311+G(d,p)	9.73	7.15	-3.68	-2.02
MP2(full)/6-311G(d,p)	214.48	211.73	203.03	200.77
MP2(full)/6-311+G(d,p)	213.58	210.66	200.96	198.34

Conclusions

In this study we have investigated the geometry and stability of the TR-GpT and TR-NB binary complexes. DFT computations reveal that *trans*-stilbene skeleton in all systems studied is strictly planar. They also suggest that the optimized geometry proves favorable interactions of TR with GpT and NB. It has been found that in the most stable geometries of TR-NB systems TR is bound to the imidazole nitrogen atom and carbonyl oxygen atom of NB by strong H-bonds, whose stability is greater in water medium. The interactions studied can be described as a combination of the three most common contributions to ΔE_{stab}: the electrostatic term, dispersion attraction and repulsion as well as exchange repulsion. The calculations with the use of C-PCM model reveal that in water medium negatively charged TR-GpT complex is significantly more stable than in vacuum, while the components of TR-NB systems are less stable in water environment. The stability of the complexes studied obtained at the DFT level can be explained by electrostatic, polarization, ionic and covalent contributions to the ΔE_{stab}. However, MP2 method which includes electron correlation effects has allowed proper description of the dispersion energy component of the ΔE_{stab}. We have shown that TR strongly bonds with negatively charged GpT dinucleotide and exhibits the ability to break the 3′-5′ phosphodiester bond. The findings obtained explain sufficiently the experimental data and give insight into theoretical explanation of chemopreventive and antiproliferative activity of TR. In conclusion, we hope that this work contributes helpful information on the TR interactions with GpT and NB. Furthermore, we are convinced that the results obtained will be useful for many experimenters who study anticancer and antiproliferative properties of TR. Additionally, to clarify the model of inhibition of topoisomerase I by TR further calculations are needed.

Table 11 The computed stabilization energies ΔE_{stab} [kcal mol^{-1}] and ΔE_{stab} + BSSE [kcal mol^{-1}] for the most stable geometries of TR-3-O-NB complexes at B3LYP/6-311G(d,p) level in vacuum and water medium

Complex	ΔE_{stab} (vacuum)	ΔE_{stab} +BSSE (vacuum)	ΔE_{stab} (water medium)	ΔE_{stab} + BSSE (water medium)
TR-3-O-A	13.45	11.44	4.57	2.20
TR-3-O-G	15.88	12.71	4.43	3.12
TR-3-O-C	10.35	8.03	3.91	1.89
TR-3-O-T	11.15	9.44	3.73	1.63

Acknowledgments We gratefully acknowledge the Supercomputing Poznań Networking for support Grant No. 60 "Investigation of the biophysicochemical properties of *trans*-resveratrol". The authors are very much indebted to MSc. Maria Spychalska for linguistic assistance and to Professor Jerzy Konarski for many valuable suggestions.

References

1. Jang M, Cai L, Udeani GO, Slowing KV, Thomas CF, Beecher CW, Fong HH, Farnsworth NR, Kinghorn AD, Mehta RG, Moon RC, Pezutto JM (1997) Cancer chemopreventive activity of resveratrol, a natural product derived from grapes. Science 275:218–220
2. Bertilli AA, Giovannini L, Gianessi D, Migliori M, Bernini W, Fregoni M, Bertilli A (1995) Antiplatelet activity of synthetic and natural resveratrol in red wine. Int J Tissue React 17:1–3
3. Uenobe F, Nakamura S, Miyazama M (1997) Antimutagenic effect of resveratrol against Trp-P-1. Mutat Res 373:197–200
4. Burkitt MJ, Duncan J (2000) Effects of *trans*-resveratrol on copper-dependent hydroxyl-radical formation and DNA damage: evidence for hydroxyl-radical scavenging and a novel, glutathione-sparing mechanism of action. Arch Biochem Biophys 381:253–263
5. Orallo F, Alvarez E, Carnina M, Leiro JM, Gomez E, Fernandez P (2004) The possible implication of *trans*-resveratrol in the cardioprotective effects of long-term moderate wine consumption. Mol Pharmacol 61:294–302
6. Szewczuk LM, Forti L, Stivala LA, Penning TM (2004) Resveratrol is a peroxidase-mediated inactivator of COX-1 but not COX-2: a mechanistic approach to the design of COX-1 selective agents. J Biol Chem 279:22727–22737
7. Fontecave M, Lepoivre M, Elleingang E, Gerez C, Guittet O (1998) Resveratrol, a remarkable inhibitor of ribonucleotide reductase. FEBS Lett 421:277–279
8. Sun NJ, Woo SH, Cassady JM, Snapka RM (1998) DNA polymerase and topoisomerase II inhibitors from *Psoralea corylifolia*. J Nat Prod 61:362–366
9. Frankel EN, Waterhouse AL, Kisella JE (1993) Inhibition of human LDL oxidation by resveratrol. Lancet 341:1103–1104
10. Belguendouz L, Fremont L, Linard A (1997) Resveratrol inhibits metal ion-dependent and independent peroxidation of porcine low-density lipoproteins. Biochem Pharmacol 53:1347–1355
11. Colin D, Lancon A, Delmas D, Lizard G, Abrossinow J, Kahn E, Jannin B, Latruffe N (2008) Antiproliferative activities of resveratrol and related compounds in human hepatocyte derived HepG2 cells are associated with biochemical cell disturbance revealed by fluorescence analyses. Biochimie 90:1674–1684
12. Pozo-Guisado E, Alvarez-Barrientos A, Mulero-Navarro S, Santiago-Josefat B, Fernandez-Salguero P (2002) The antiproliferative activity of resveratrol results in apoptosis in MCF-7 but not in MDA-MB-231 human breast cancer cells: cell-specific alteration of the cell cycle. Biochem Pharmacol 64:1375–1386
13. Roccaro AM, Leleu X, Sacco A, Moreau A-S, Hatjiharissi E, Jia X, Xu L, Ciccarelli B, Patterson CJ, Ngo HT, Russo D, Vacca A, Dammacco F, Anderson KC, Ghobrial IM, Treon SP (2008) Resveratrol exerts antiproliferative activity and induces apoptosis in Waldenström's macroglobulinemia. Clin Cancer Res 14:1849–1858
14. Hsieh TC (2009) Antiproliferative effects of resveratrol and the mediating role of resveratrol targeting protein NQO2 in androgen receptor-positive, hormone-non-responsive CWR22Rv1 cells. Anticancer Res 29:3011–3017
15. Kang JH, Park YH, Choi SW, Yang EK, Lee WJ (2003) Resveratrol derivatives potently induce apoptosis in human promyelocytic leukemia cells. Exp Mol Med 35:467–474
16. Zhou H-B, Chen J-J, Wang W-X, Cai J-T, Du Q (2005) Anticancer activity of resveratrol on implanted human primary gastric carcinoma cells in nude mice. World J Gastroenterol 11:280–284
17. Frisch MJ, Trucks GW, Schlegel HB, Scuseria GE, Roob MA, Cheeseman JR, Montgomery JA, Vreven T, Kudin KN, Burant JC, Millam JM, Iyengar SS, Tomasi J, Barone V, Menucci B, Cossi M, Scalmani G, Rega N, Petersson GA, Nakatsuji H, Hada M, Ehara M, Toyota K, Fukuda R, Hasegawa J, Ishida M, Nakajima T, Honda Y, Kitao O, Nakai H, Klene M, Li X, Knox JE, Hratchian HP, Cross JB, Bakken V, Adamo C, Jaramillo J, Gomperts R, Stratmann RE, Yazyev O, Austin AJ, Cammi R, Pomelli C, Ochterski JW, Ayala Y, Morokuma K, Voth GA, Salvador P, Dannenberg JJ, Zakrzewski VG, Dapprich S, Daniels AD, Strain MC, Farkas O, Malick DK, Rabuck AD, Raghavachari K, Foresman JB, Ortiz JV, Cui Q, Baboul AG, Clifford S, Ciosłowski J, Stefanov BB, Liu G, Liashenko A, Piskorz P, Komaromi I, Martin RL, Fox DJ, Keith T, Al-Laham MA, Peng CY, Nanayakkara A, Challacombe M, Gill PMW, Johnson B, Chen W, Wong MW, Gonzalez C, Pople JA (2004) Gaussian 03, revision C.02. Gaussian Inc, Wallingford, CT
18. Lee C, Yang W, Parr RG (1988) Development of the Colle-Salvetti correlation-energy formula into a functional of the electron density. Phys Rev B 37:785–789
19. Pavelka M, Shukla MK, Leszczyński J, Burda JV (2008) Theoretical study of hydrated copper(II) interactions with guanine: a computational density functional theory study. J Phys Chem A 112:256–267
20. Burda JV, Pavelka M, Šimánek M (2004) Theoretical model of copper Cu(I)/Cu(II) hydration. DFT and ab initio quantum chemical study. J Mol Struct THEOCHEM 683:183–193
21. Boys SF, Bernard F (1970) The calculation of small molecular interactions by the differences of separate total energies. Some procedures with reduced errors. Mol Phys 19:553–566
22. Mikulski D, Szeląg M, Molski M, Górniak R (2010) Quantum-chemical study on the antioxidation mechanisms of *trans*-resveratrol reactions with free radicals in the gas phase, water and ethanol environment. J Mol Struct THEOCHEM 951:37–48
23. Cossi M (2003) Energies, structures, and electronic properties of molecules in solution with the C-PCM solvation model. J Comput Chem 24:669–681
24. Ben-Naim A, Marcus Y (1984) Solvation thermodynamics nonionic solutes. J Chem Phys 81:2016–2027
25. Gupta M, Fujimori A, Pommier Y (1995) Eukaryotic DNA topoisomerase I. Biochim Biophys Acta 1262:1–14
26. Fan Y, Weinstein JN, Kohn KW, Shi LM, Pommier Y (1998) Molecular modeling studies of the DNA-topoisomerase I ternary cleavable complex with camptothecin. J Med Chem 41:2216–2226
27. Riahi S, Eynollahi S, Ganjali MR, Norouzi P (2010) Computational studies on effects of Efavirenz as an anticancer drug on DNA: application in drug design. Int J Electrochem Sci 5:815–827
28. Hobza P, Šponer J, Reschel T (1995) Density functional theory and molecular clusters. J Comput Chem 16:1315–1325
29. Xu X, Goddard WA III (2004) The X3LYP extended density functional for accurate descriptions of nonbond interactions, spin states, and thermochemical properties. Proc Natl Acad Sci USA 101:2673–2677